Experimental Investigation of Bed Shear Stress Distribution in Spatially Varied Flow

Zaid Hamid Hasan*, Mohammed A Alabas

Department of Civil Engineering, University of Babylon, Hillah 51002, Iraq

Corresponding Author Email: Zaid.Hussein.engh335@student.uobabylon.edu.iq

ABSTRACT

Boundary shear stress plays a critical role in open-channel hydraulics, controlling momentum exchange with boundaries, sediment transport, and hydraulic resistance. This paper experimentally investigates the distribution of boundary shear stress in spatially varied flow (SVF) with increasing discharge caused by lateral inflows. A full-scale roadway model (6.2 m × 2 m × 1.5 m) was constructed with adjustable slopes, base discharges of 10 and 50 m³/hr, and lateral inflows (nozzles discharges) of 5 and 12 m³/hr. Flow depths were measured using ultrasonic sensors, while velocity gradients in the viscous sublayer were captured with a Laser Doppler Velocimeter (LDV) to compute local shear stresses. A total of 216 experiments were performed at 54 measurement points across multiple longitudinal sections. Results demonstrate that normalized bed shear stress exhibits minimal variation at the upstream and downstream boundaries but decreases transversely from the model centerline to the walls within the inflow zone. Negative shear stresses were observed near nozzle entry points, indicating local flow reversal due to jet impingement. The influence of lateral inflow was strongest at low base discharges and diminished at higher discharges, highlighting the interaction between main channel flow and turbulence induced by inflow jets.

1. INTRODUCTION

Boundary shear stress is a central concept in open-channel hydraulics, as it governs momentum exchange between flowing water and channel boundaries, influences sediment transport, and dictates hydraulic resistance. Accurate estimation of bed shear stress is thus essential for addressing a range of environmental flow challenges, including water quality, habitat modelling, and the protection of fluvial and coastal infrastructure [1]. Boundary shear stress as the tangential force per unit area exerted by the fluid on the channel bed and sidewalls, boundary shear stress has wide-ranging implications for river morphology, flood risk management, and engineering design. Understanding how shear stress is distributed along channel boundaries is critical for accurately predicting erosion, stability of hydraulic structures, and efficiency of conveyance systems [2, 3].

In practice, open-channel flows are seldom uniform. Variations in geometry, inflows, and turbulence intensity lead to significant spatial heterogeneity in boundary shear stress [4, 5]. The theoretical formulation and experimental investigation of spatially varied flow with increasing discharge have been of interest to many researchers in the fields of hydraulics, hydrology, and soil science. Theoretical studies in this area have been mainly based on a one-dimensional analysis of spatially varied flow. In this approach, the principle of linear momentum together with the equation of continuity have been used to develop an equation for variation of the water surface elevation [6-9].

Bed shear stress (τ_b) in open channels can be determined through several complementary approaches (as shown in Table 1). Direct methods, such as the Preston tube, shear plate, and Laser Doppler Velocimetry (LDV), measure the shear or near-bed velocity field with high precision. LDV, in particular, provides instantaneous point-velocity data that enable evaluation of the friction velocity (u*) and subsequent calculation of $\tau_b = \rho\, u^*$ [10].

Indirect hydraulic methods including the slope–depth and momentum-balance approaches estimate τ_b from overall flow parameters such as slope, hydraulic radius, and discharge distribution. Empirical relations, for example the Darcy–Weisbach or Manning formulations, express τ_b as a function of the mean velocity and friction factor, while sediment-based or CFD methods infer it from bed-load initiation or numerical flow simulation [11].

Recent advances in open-channel hydraulics have emphasized the importance of understanding how shear stress responds to flow non-uniformity, turbulence generation, and local inflow conditions. Modern studies have shown that lateral inflow can significantly modify near-bed flow structures, induce localized shear concentration, and create regions of flow reversal that cannot be captured by depth-averaged theories alone [12].

Table 1. The summary of boundary shear stress determination methods

Method Type	Description	Key Equation	Accuracy	Application	Reference
Preston tube	Local pressure-based measurement	$\tau_b = \rho u^{*2}$	High	Smooth bed, Lab flumes	[6]
Slope–Depth	Uniform flow relation	$\tau_b = \gamma RS$	Moderate	Straight channels	[9, 13]
LDV/PIV	Velocity profile fitting	$\tau_b = \rho u^{*2}$	Very High	Research-grade studies	[10]
Friction factor	Empirical relations	$\tau_b = f\rho V^2/8$	Moderate	Wide range	[11, 6]
Velocity Distribution Method	From velocity gradient at wall using du/dy	$\tau_b = \rho v(du/dy)$	Very High	Research-grade velocity data	[14]
Shields criterion	Sediment incipient motion	$\tau_{bx} = \theta_c\,[(\rho_s - \rho)\,gd]$	Moderate	Movable beds	[15]
Momentum balanced method	Non-uniform flow analysis	$\tau_b = [\rho gAS - d(\rho QV)/dx]/P$	High	SVF with lateral inflow	[16]
Energy Gradient Method	Derived from head loss between two sections	$\tau_b = \rho gR(\Delta h/\Delta x)$	Moderate	Gradually varied flow	[17]

Among these, the LDV technique was adopted in the present experimental study owing to its superior spatial and temporal resolution and its ability to capture velocity gradients within the near-bed region of the laboratory flume. The resulting τ_b values are therefore grounded in direct physical measurement, ensuring high reliability in characterizing boundary resistance and flow behavior under spatially varied conditions. This study presents an experimental investigation of the distribution of bed shear stress in a channel subjected to lateral inflow. In such conditions, the discharge increases progressively along the channel length, representing a form of SVF with increasing discharge. In this study, the average boundary shear stresses were first determined, and the corresponding friction factors were then estimated using the established formulation for SVF with increasing discharge [6]. Local boundary shear stresses were then calculated based on the assumption of a linear velocity distribution within the viscous sublayer, so the local boundary shear stress can be obtained as follows in Eq. (1) [18, 19]:

$$\tau_{\circ x} = \mu\frac{du}{dy} \tag{1}$$

where, $\tau_{\circ x}$: local boundary shear stress, μ: dynamic viscosity; y: distance from the channel bed; and u: mean longitudinal local velocity.

In wall coordinates, the velocity distribution within the viscous sublayer can be expressed using the following relation in Eq. (2):

$$U^+ = Y^+ \tag{2}$$

where, Y^+: yu^*/υ; and U^+: u/u^* with $u^* = (\tau_{\circ x}/\rho)^{1/2}$ with ρ being the mass density of the fluid [14, 15, 20-22].

Understanding how bed shear stress behaves under spatially varied flow with increasing discharge is essential for accurately characterizing hydraulic resistance, sediment mobility, and flow transitions in systems receiving lateral inflow. Existing formulations commonly describe SVF using depth-averaged or one-dimensional approaches, yet these methods do not fully capture the localized effects produced by inflow jets, such as transverse stress variation, near-bed velocity gradients, or the occurrence of stress reversal. Detailed experimental data, particularly those obtained using high-resolution LDV measurements under controlled full-scale conditions, are therefore valuable for improving the description of shear stress distribution in practical applications. In this context, the present study conducts a comprehensive experimental investigation in a full-scale roadway model to quantify bed shear stress behavior in the presence of lateral inflow and increasing discharge, providing a refined depiction of how shear stress evolves both longitudinally and laterally within the flow field.

2. EXPERIMENTAL PROCEDURE

Tests were conducted in a 1:1 scale model of a roadway measuring 6.2 m long, 2 m wide, and 1.5 m high. Point velocities were measured with a Laser Doppler Velocimeter (LDV) in Figure 1, and water depths were recorded with an Ultrasonic Water Level (UWL) sensor (Figure 2). The model is able to simulate a road with longitudinal slope by using 6 hydraulic jacks mounted under the legs of the model. Pump systems feed discharge to a tank, and a motorized slide valve controls the supplied discharge to the model.

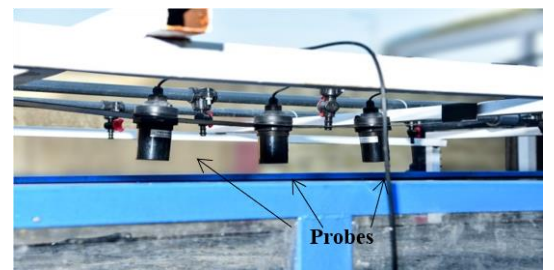**Figure 1.** Experimental model equipment

Figure 2. Probe of UWL

To simulate the SVF type that occurs in roads, the model was equipped with a main flow through the tanks and a lateral inflow via 4 nozzles, as shown in Figure 3. Discharge measurement is done by a calibrated flowmeter and the flow reaches the test area through a tank located upstream of the model. This tank provides sheet flow and a horizontal profile

to the surface water elevation and dissipates the energy of flow by using a weir at the middle of the tank [23]. With this method, the surface water level is constant across the platform's width, making it easier to approximate a uniform and steady flow in this road model, as shown in Figure 4. The model is able to simulate the roadway with the studied parameters, which are varied throughout this paper according to the following.

- Supplied discharge (base flow) = 10 and 50 m^3/hr
- Lateral inflow (nozzle discharge) = 5 and 12 m^3/hr
- Longitudinal slope (S_L) = 1.5%
- Number of measurement point = 54
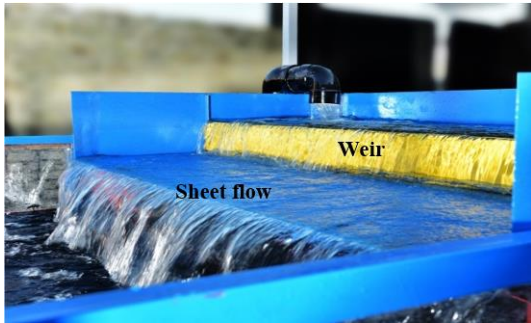
Figure 3. Sheet flow in the model
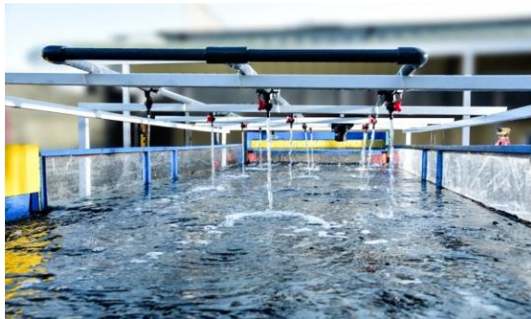
Figure 4. Nozzles in the model

2.1 Experimental error and uncertainty

The accuracy and reliability of the experimental results are fundamentally influenced by the precision of the measuring instruments and the consistency of the recorded data. All hydraulic measurements in this study were subjected to both instrumental and repeatability uncertainties, which were systematically analyzed to assess their potential influence on the computed hydraulic parameters, including water depth, velocity, discharge, Reynolds number (Re), Froude number (Fr), and the Darcy–Weisbach friction factor (*f*).

2.1.1 Instrumental uncertainties

Instrumental uncertainty arises from the inherent limitations and calibration accuracy of the devices employed in the hydraulic experiments. The principal measuring instruments included a LDV for point velocity measurements, an UWL sensor for determining flow depth, a flow meter for monitoring the base discharge, and a V-notch weir for calibration and validation of discharge measurements. The nominal accuracies of these instruments are presented in Table 2, which summarizes the measurement precision and operating remarks for each device.

Table 2. Specifications and nominal accuracies of the instruments used for hydraulic measurements

Instrument	Measured Variable	Accuracy	Remarks
LDV	Local velocity (U)	± 1% of reading	Depth-wise velocity measurements
UWL	Water depth (h)	± 1 mm	Calibrated before each run
Flow Meter	Base discharge (Q)	± 1%	Continuous flow monitoring
V-Notch Weir	Discharge (Q)	Cd ± 2%, H ± 1 mm	Used for cross-checking flow rate

2.1.2 Repeatability uncertainty

Repeatability uncertainty was evaluated by performing multiple readings at each measurement location under steady-state flow conditions. The standard deviation of these repeated measurements was used as an indicator of random variability in the data. This approach was particularly relevant to LDV velocity measurements, where instantaneous flow fluctuations may influence the readings. Averaging several measurements under identical conditions effectively minimized random errors and improved the overall reliability of the experimental dataset.

3. RESULT AND DISCUSSION

A set of 216 experiments are conducted to examine the boundary shear stress in the model at the measurement points (P) shown in Figure 5.
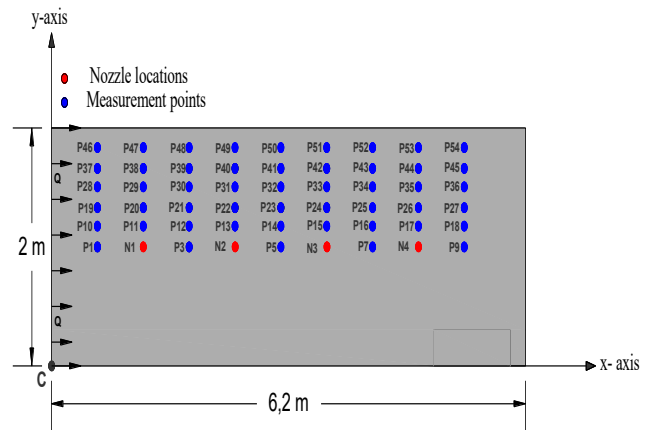

Figure 5. Distribution of measurement points in the model

Measurement points were taken on one side of the model because the flow conditions were symmetrical across the centerline of the model. If we consider point (C) to be the origin point (0,0) for the rest of the points, the coordinates of the measurement points are listed in Table 3.

Velocities near the channel bed were measured by positioning the laser probe adjacent to the sidewall, allowing the laser beam to be guided horizontally toward the measurement zone. This setup made it possible to obtain velocity readings very close to the bed surface. At a few measurement locations, one or two data points near the boundary were excluded from the least-squares analysis, as they were identified as outliers and likely affected by noise in the signal.

To verify the accuracy of the experimental setup and instrumentation, velocity profiles were obtained along the channel centerline at a distance of 4 m from the upstream end. Measurements were conducted under two steady discharges of 10, and 50 m³/hr in the absence of spatially varied (SV), Lateral inflow (nozzle discharge). The experimental conditions associated with these baseline tests are summarized in Table 4.

Table 3. Coordinate of the measurement points

Point Measurement Information			Point Measurement Information		
Point name	x (m)	y (m)	Point name	x (m)	y (m)
P1	0.6	1	P28	0.6	1.495
P2, N1	1.2	1	P29	1.2	1.495
P3	1.8	1	P30	1.8	1.495
P4, N2	2.4	1	P31	2.4	1.495
P5	3	1	P32	3	1.495
P6, N3	3.6	1	P33	3.6	1.495
P7	4.2	1	P34	4.2	1.495
P8, N4	4.8	1	P35	4.8	1.495
P9	5.4	1	P36	5.4	1.495
P10	0.6	1.165	P37	0.6	1.66
P11	1.2	1.165	P38	1.2	1.66
P12	1.8	1.165	P39	1.8	1.66
P13	2.4	1.165	P40	2.4	1.66
P14	3	1.165	P41	3	1.66
P15	3.6	1.165	P42	3.6	1.66
P16	4.2	1.165	P43	4.2	1.66
P17	4.8	1.165	P44	4.8	1.66
P18	5.4	1.165	P45	5.4	1.66
P19	0.6	1.33	P46	0.6	1.825
P20	1.2	1.33	P47	1.2	1.825
P21	1.8	1.33	P48	1.8	1.825
P22	2.4	1.33	P49	2.4	1.825
P23	3	1.33	P50	3	1.825
P24	3.6	1.33	P51	3.6	1.825
P25	4.2	1.33	P52	4.2	1.825
P26	4.8	1.33	P53	4.8	1.825
P27	5.4	1.33	P54	5.4	1.825

Table 4. Experimental results without SV inflow

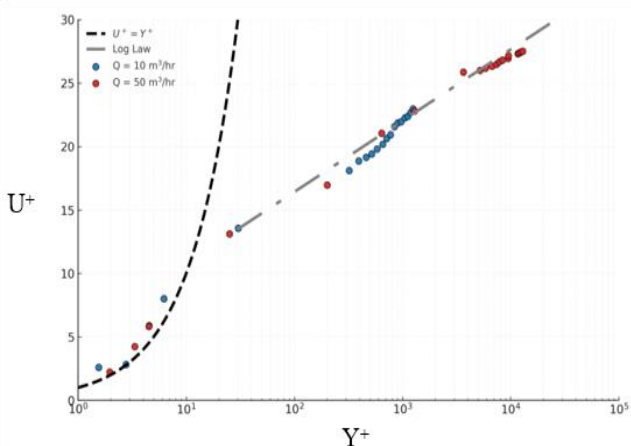| Base Discharge (m³/hr)	Mean Velocity U (m/s)	Flow Depth (m)	S_L	Fr	Re	u_* (m/s)
10	0.27	0.007	0.015	1.05	7210	0.031
50	0.67	0.028	0.015	1.31	71171	0.062

Figure 6. Comparison of experimental data with the universal velocity profile

Baseline velocity distributions were first obtained in the absence of spatially varied (SV) inflow in order to provide a reference for identifying the influence of nozzle-induced inflow in subsequent experiments. Figure 6 presents the two velocity profiles measured, expressed in wall coordinates U^+ and Y^+. All measurements were conducted with a Manning roughness coefficient of n = 0.016, representing a rough asphalt bed [24, 25]. The Figure also includes the logarithmic velocity distribution equation, which characterizes the inertial sublayer region.

Figure 6 shows that the results of this study are in close agreement with the equation proposed by Nezu and Rodi [26] confirming that both the flume setup and the measurement instruments were properly calibrated and suitable for experiments involving lateral inflow.

Figures 7 to 24 illustrate the distribution of the normalized bed shear stress ($\tau_b / \overline{\tau_\circ}$) across the channel width, where $\overline{\tau_\circ}$ represents the average shear stress along the wetted perimeter.
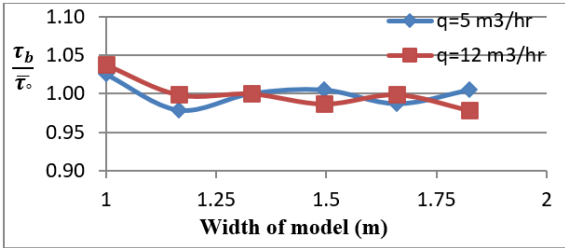

Figure 7. Variation of normalized bed shear stress across the model width at x = 0.6 m, and Q = 10 m³/hr
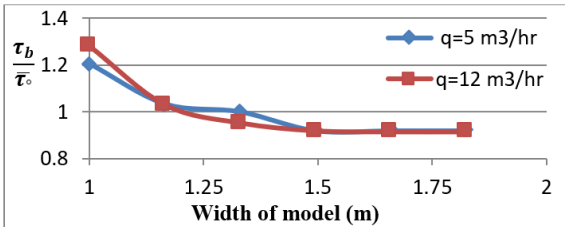

Figure 8. Normalized τ_b across the model width at x = 1.2 m, and Q = 10 m³/hr
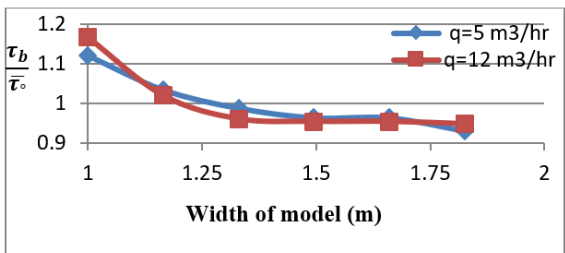

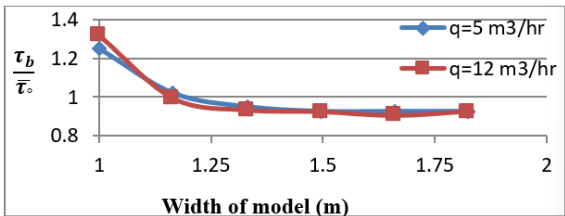**Figure 9.** Normalized τ_b across the model width at x = 1.8 m, and Q = 10 m³/hr

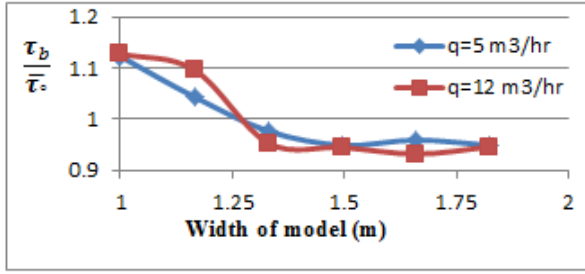**Figure 10.** Normalized τ_b across the model width at x = 2.4 m, and Q = 10 m³/hr

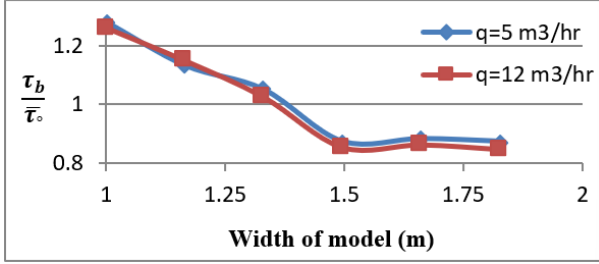**Figure 11.** Normalized τ_b across the model width at x = 3 m, and Q = 10 m³/hr

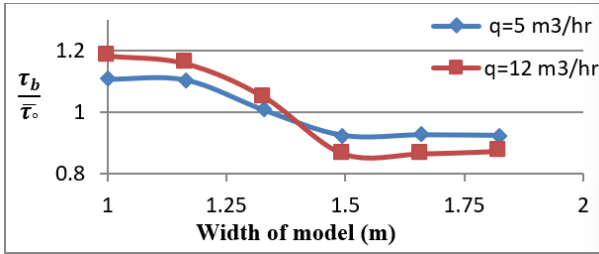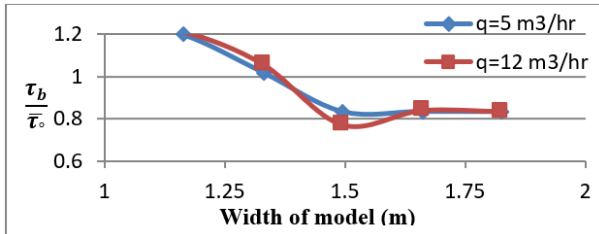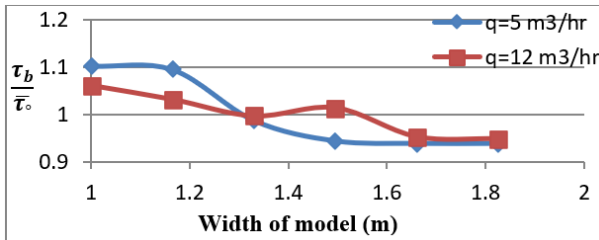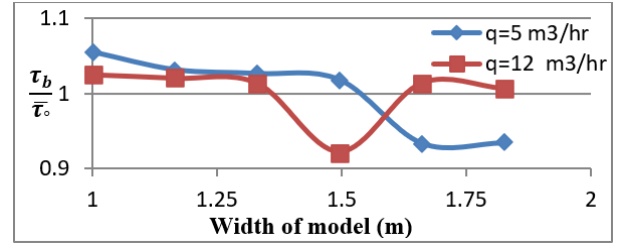**Figure 12.** Normalized τ_b across the model width at x = 3.6 m, and Q = 10 m³/hr

Figure 13. Normalized τ_b across the model width at x = 4.2 m, and Q = 10 m³/hr

Figure 14. Normalized τ_b across the model width at x = 4.8 m, and Q = 10 m³/hr

Figure 15. Normalized τ_b across the model width at x = 4.8 m, and Q = 10 m³/hr

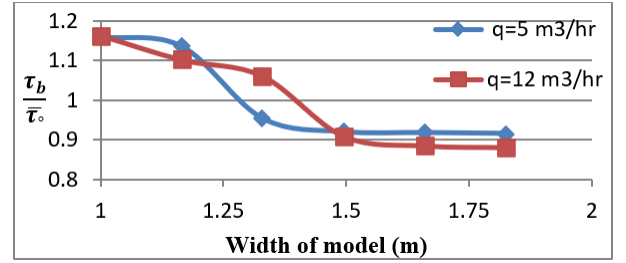**Figure 16.** Normalized τ_b across the model width at x = 0.6 m, Q = 50 m³/hr

Figure 17. Normalized τ_b across the model width at x = 1.2 m, Q = 50 m³/hr
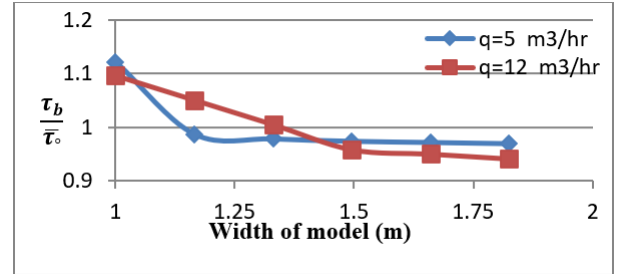

Figure 18. Normalized τ_b across the model width at x = 1.8 m, Q = 50 m³/hr
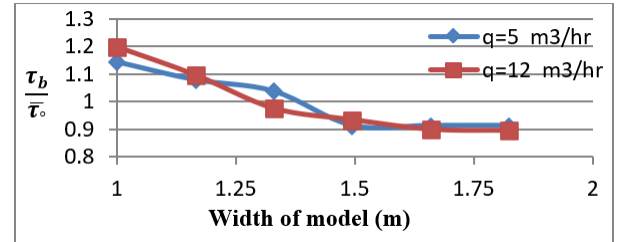

Figure 19. Normalized τ_b across the model width at x = 2.4 m, Q = 50 m³/hr
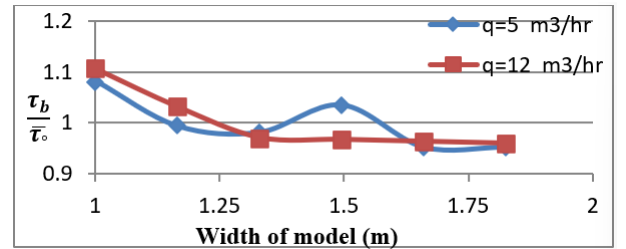

Figure 20. Normalized τ_b across the model width at x = 3 m, Q = 50 m³/hr
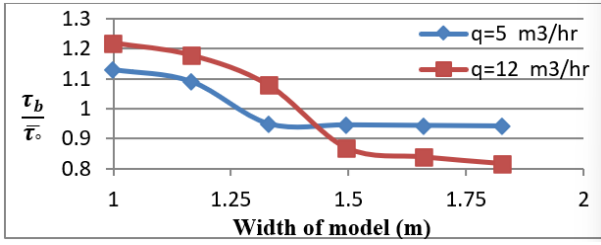
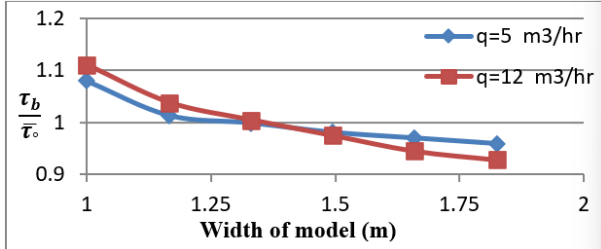**Figure 21.** Normalized τ_b the model width at x = 3.6 m, Q = 50 m³/hr

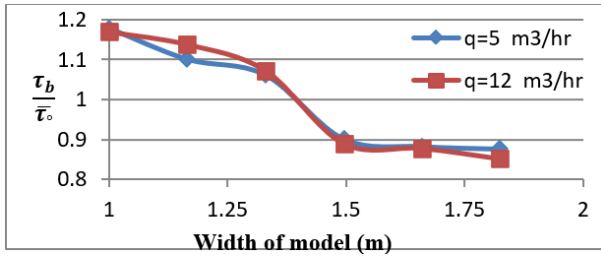**Figure 22.** Normalized τ_b across the model width at x = 4.2 m, Q = 50 m³/hr

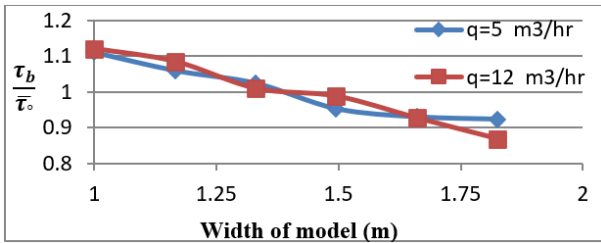**Figure 23.** Normalized τ_b across the model width at x = 4.8 m, Q = 50 m³/hr

Figure 24. Normalized τ_b across the model width at x = 5.4 m, Q = 50 m³/hr

Figures 7 and 24 demonstrate that at x = 0.6 m and x = 5.4 m, the normalized bed shear stress exhibits only minor transverse variation when compared with the remaining measurement sections. The section at x = 0.6 m lies upstream of the nozzle (N1), at x = 5.4 m corresponds to downstream boundary of the lateral inflow zone. Notably, even with 140% increase in the discharge from each nozzle from q=5 to 12 m³/hr, no discernible influence of lateral inflow on the ($\tau_b / \overline{\tau_\circ}$) was detected at measurement locations.

For the remaining cross sections shown in the figures, the ($\tau_b/\overline{\tau_\circ}$) decreases with increasing streamwise distance (y). At a given cross section, the ($\tau_b / \overline{\tau_\circ}$) reaches its maximum at the model centerline and decreases progressively toward the sidewalls. The transverse variation is most pronounced up to approximately half the distance between the model centerline and the model wall. Further downstream, however, this lateral

variation becomes less significant, indicating a more uniform distribution of bed shear stress across the model width.

It was observed that the ($\tau_b/\overline{\tau_\circ}$) does not exhibit significant variation along the model length. A slight increase in normalized bed shear stress may be anticipated in the downstream direction due to the gradual rise in velocity; however, this trend appears to be influenced by the presence of lateral inflow at different measurement sections. A comparison of nozzle discharges (q = 5 and 12 m³/hr) shows that a 140% increase in lateral inflow has not produced a substantial effect on the overall distribution of normalized bed shear stress.

To provide a clearer understanding of bed shear stress behavior, the experimentally measured values between and beneath the nozzle positions are presented in Figures 25 to 36. These results illustrate the spatial variation of shear stresses along the bed in relation to the nozzle inflow.
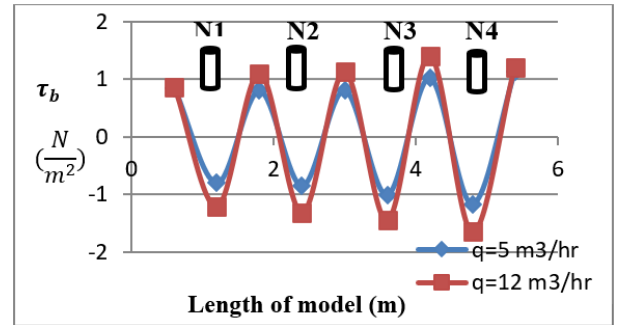

Figure 25. τ_b distribution along the model length at y = 1 m, Q = 10 m³/hr, showing the effect of nozzles N1-N4

Figure 26. τ_b distribution along the model length at y = 1.165 m, Q = 10 m³/hr

Figure 27. τ_b distribution along the model length at y = 1.33 m, Q = 10 m³/hr

The results indicate that along the model centerline, the measured bed shear stress decreases progressively as the nozzle region is approached. Slightly upstream of the nozzle axis, the stresses become negative, before rising to peak value downstream of the nozzle. A similar pattern is evident for

successive downstream nozzles, as shown in Figures 25 and 31. The occurrence of negative bed shear stresses in these regions signifies local flow reversal. This behavior suggests that the nozzle jet impinges on the channel bed and subsequently spreads radially within the surrounding region. At the stagnation point, the bed shear stress reduces to zero.

Figure 28. τ_b distribution along the model length at y = 1.495 m, Q = 10 m³/hr

Figure 29. τ_b distribution along the model length at y = 1.66 m, Q = 10 m³/hr

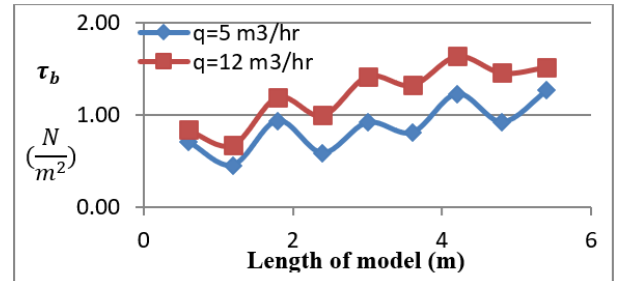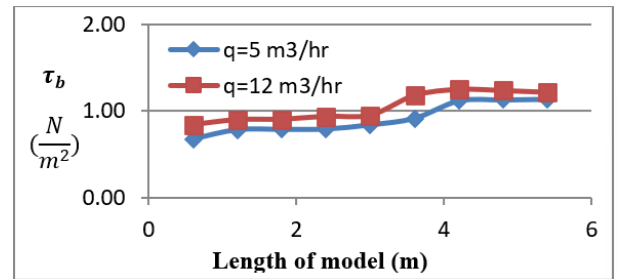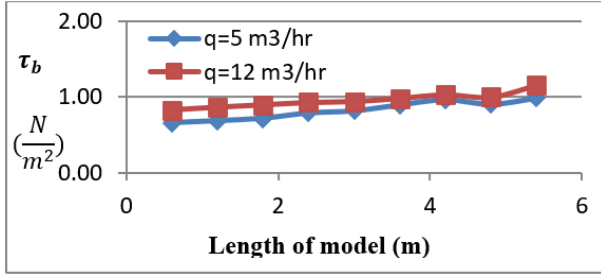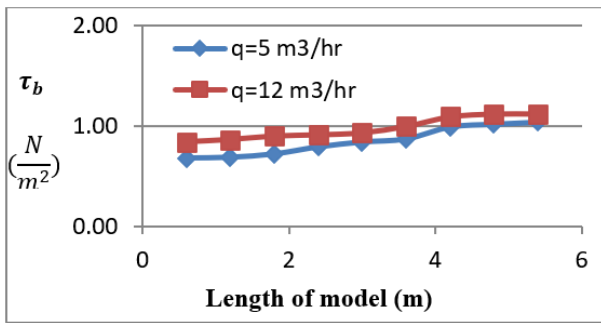**Figure 30.** τ_b distribution along the model length at y = 1.825 m, Q = 10 m³/hr

Figure 31. τ_b distribution along the model length at y = 1 m, Q = 50 m³/hr

The influence of nozzle discharge on bed shear stress was observed to extend up to y = 1.165 m. This effect intensifies as the nozzle discharge increases from q = 5 to 12 m³/hr. The influence is most evident under low base discharge conditions (Q = 10 m³/hr), as illustrated in Figure 26, and nearly vanishes when the base discharge reaches Q = 50 m³/hr. This behavior is physically consistent: with increasing discharge, both the flow depth and velocity rise, allowing the main flow to overcome the turbulence induced by the nozzle jets, thereby restoring the bed shear stress distribution to its natural state, as depicted in Figure 32.

The interaction between the main model discharge and the nozzle jets causes the inflow to deflect, shifting the impingement region downstream of the jet. This region corresponds to the location where the maximum bed shear stress is observed. Moving laterally away from the nozzle region toward the sidewalls of the model, the variation in bed shear stress decreases. This indicates that the influence of lateral inflow on bed shear stress is strongest directly beneath the nozzle entry points and diminishes at positions farther from the jet.

Figure 32. τ_b distribution along the model length at y = 1.165 m, Q = 50 m³/hr

Figure 33. τ_b distribution along the model length at y = 1.33 m, Q = 50 m³/hr

Figure 34. τ_b distribution along the model length at y = 1.495 m, Q = 50 m³/hr

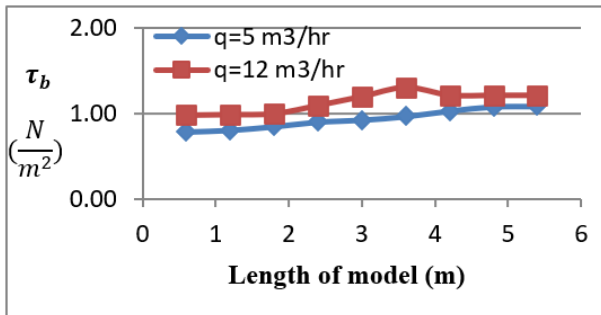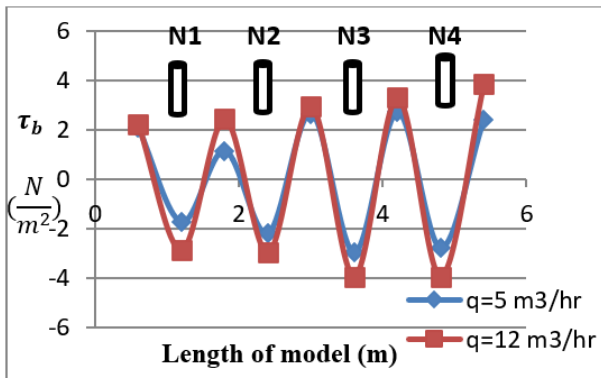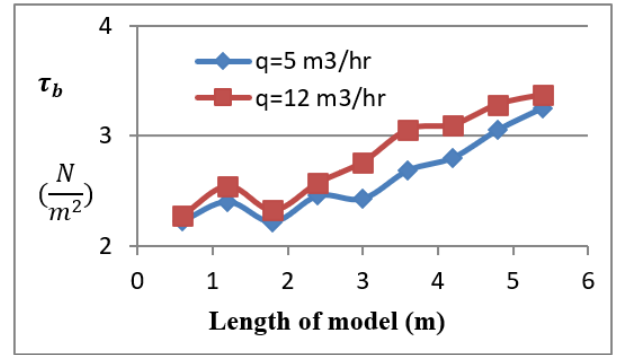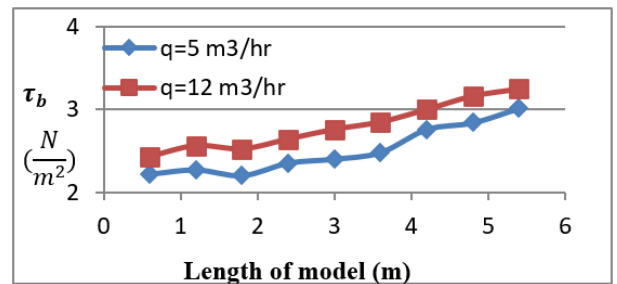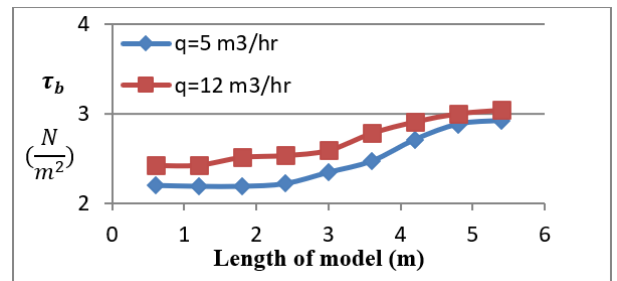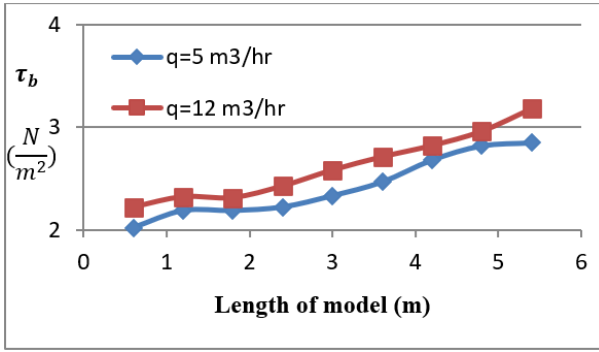**Figure 35.** τ_b distribution along the model length at y = 1.66 m, Q = 50 m³/hr

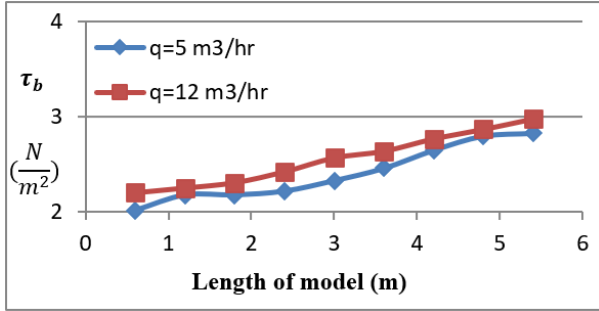**Figure 36.** τ_b distribution along the model length at y = 1.825 m, Q = 50 m³/hr

4. STATISTICAL ANALYSIS

In spatially varied flow (SVF) with increasing discharge, τ_b varies both longitudinally and vertically due to the influence of lateral inflow, changes in slope, and local turbulence structures. Understanding these variations is essential for accurately describing the hydraulic behavior of complex open-channel systems [10].

Dimensional analysis provides a powerful and systematic approach for correlating τ_b with the governing hydraulic, geometric, and fluid properties. By applying the Buckingham π-theorem, τ_b can be related to a set of nondimensional parameters such as the Reynolds number (Re), Froude number (Fr), relative flow depth (y/h), discharge ratio (q/Q), longitudinal slope (S_L), and streamwise position (x/h). These dimensionless groups encapsulate the combined effects of geometry, fluid mechanics, and flow regime, allowing the generalization of laboratory results to broader hydraulic conditions [9, 16]. Therefore, the present study employs a boundary-oriented dimensional analysis to establish relationships between τ_b and the controlling parameters of spatially varied flow with increasing discharge. This

formulation enables the development of empirical expressions that accurately capture the influence of slope, inflow, and geometric scaling on boundary shear stress in controlled laboratory environments.

Building on the dimensional analysis, the reliability of the proposed relationships was evaluated using established statistical performance indicators. The bed shear stress was expressed in Eq. (3), as a function of key hydraulic and geometric parameters:

$$\tau_b = \alpha \, \rho \, V^2 \, (q/Q)^a \, (x/h)^b \, (y/h)^c \, (h/b)^d \, (ks/h)^e \, (S_L)^f \, (Fr)^g \, (Re)^i \tag{3}$$

The empirical relationship for bed shear stress (τ_b) was developed using SPSS and Multiple Nonlinear Regression (MNLR), a widely adopted approach in hydraulic modeling to quantify the influence of flow and geometric parameters to quantify the influence of flow and geometric parameters [6, 9, 16, 27]. The coefficients (α, a, b, c, d, e, f, g, i) were determined experimentally based on laboratory data following the principles of turbulent flow similarity. Table 5 displays the statistical importance of each parameter category.

Table 5. Regression coefficient values

Coefficient	α	a	b	c
Value	0.0145	-0.056	0.126	5.16
Coefficient	d	e	f	g
Value	- 6.00	-11.43	17.78	-18.60

Figure 37 compares the predicted and observed bed shear stress values (τ_0).
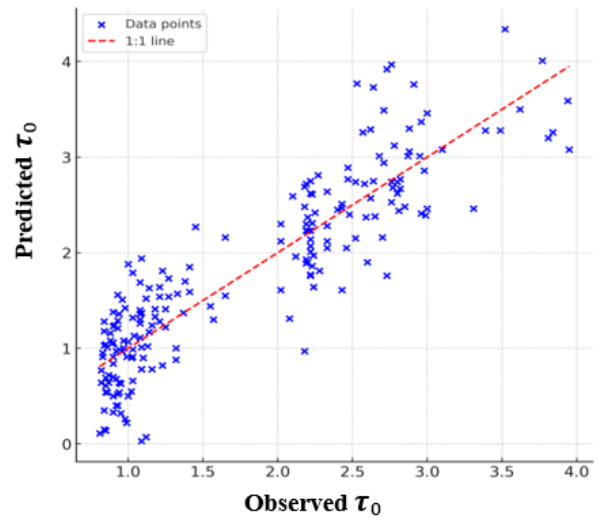
Figure 37. Observed versus predicted τ_0

Table 6. Quantitative statistical coefficients to investigate model accuracy

Metric	Obtained Value	Optimal Value	Interpretation
R^2	0.7368	1, -1	Explains ~73.7% of variability in observed τ_b.
d	0.9380	1	Shows strong agreement between observed and predicted τ_b values.
MAE	0.347	0	Represents small average deviation between predicted and observed data.
NSE	0.737	1	Indicates that the model performs significantly better than the mean of observations.

The performance of the proposed regression model was evaluated using standard statistical indicators recommended in hydrological and hydraulic modeling studies [28, 29]. These metrics—R^2, d, MAE, and NSE—are essential for quantifying model accuracy, consistency, and predictive capability, as shown in Table 6.

The regression model demonstrates reliable predictive capability for boundary shear stress under spatially varied flow conditions with increasing discharge [11, 15]. The coefficient of determination ($R^2 = 0.7368$) and Nash–Sutcliffe efficiency (NSE = 0.737) confirm a strong correlation between observed and predicted results. Moreover, the high index of agreement (d = 0.938) and low MAE (0.347) indicate that the model captures flow behavior accurately, minimizing deviations between experimental and computed τ_b values. These results are consistent with modern hydraulic studies that emphasize the role of flow resistance and channel roughness in modeling energy dissipation [17].

5. CONCLUSION

The results show that the $\tau_{\circ x}$ are strongly affected by the presence of lateral inflow, with the most pronounced variations occurring in the vicinity of the inflow entry points. Along the length of the lateral inflow zone, mean boundary shear stress and mean bed shear stress were evaluated and compared at multiple measurement locations. The findings indicate that mean boundary shear stress increases progressively from the upstream side toward the downstream end of the inflow region. Likewise, the $\overline{\tau_b}$, rises sharply as the flow approaches the lateral inflow zone and continues to increase throughout this region, reaching its highest value at the downstream edge of the inflow zone

The normalized bed shear stress ($\tau_b / \overline{\tau_\circ}$) exhibits minimal variation at the upstream section (x = 0.6 m) and at the downstream boundary (x = 5.4 m). This indicates that the influence of lateral inflow is negligible at these positions, even with a 140% increase in nozzle discharge.

At intermediate cross-sections, the normalized bed shear stress decreases with increasing streamwise distance. It reaches a maximum at the model centerline and diminishes toward the sidewalls. The transverse variation is significant up to half the distance between the centerline and the wall but becomes less pronounced further downstream, reflecting a more uniform stress distribution across the flume width.

Along the channel length, normalized bed shear stress remains relatively stable. Although a slight downstream increase might be expected due to rising velocity, this effect is weak and strongly influenced by local lateral inflows. Increasing nozzle discharge from q = 5 to 12 m³/hr did not significantly alter the longitudinal distribution of normalized bed shear stress.

Bed shear stress near the nozzles shows a characteristic pattern: it decreases approaching the nozzle, becomes slightly negative upstream of the nozzle axis, and reaches a peak immediately downstream. Negative values indicate local flow reversal caused by jet impingement on the bed, with shear stress reducing to zero at stagnation points.

The impact of nozzle inflow on bed shear stress extends up to y = 1.165 m. This influence is most evident at low base discharges (Q = 10 m³/hr) and nearly disappears at Q = 50 m³/hr. This behavior is physically consistent: higher discharges increase flow depth and velocity, allowing the main flow to suppress nozzle-induced turbulence.

Interaction between the main flow and nozzle jets causes inflow deflection, shifting the impingement zone downstream of the jets where maximum bed shear stress occurs. Moving laterally away from the nozzle region, the influence of lateral inflow weakens, indicating that its effect on bed shear stress is strongest directly beneath the nozzles.

Future research can extend the present findings by investigating the influence of additional hydraulic parameters, such as variable bed roughness, different nozzle orientations, and non-uniform slopes. Incorporating sediment transport into similar experiments would provide further insight into erosion processes associated with spatially varied flow. Numerical simulations using CFD could also complement the experimental dataset by visualizing flow structures. Expanding the full-scale model to other geometries—such as trapezoidal or compound channels—would help generalize the results for broader engineering applications.

REFERENCES

[1] Aliaga-Villagrán, J., Artini, G., Macías-Lezcano, J., Llull, T., Núñez-González, F., Aberle, J. (2025). Uncertainty analysis for direct bed shear stress measurements using shear plates. Acta Geophysica, 73: 5959-5975. https://doi.org/10.1007/s11600-025-01691-6

[2] Pradhan, A., Khatua, K.K., Sahoo, K.K., Mohanta, A., Beulah, M., Sudhir, M.R. (2024). Bed shear stress distribution across a meander path. Journal of Water and Climate Change, 15(9): 4220-4236. https://doi.org/10.2166/wcc.2024.682

[3] Aliaga, J., Aberle, J. (2024). Bed shear stress and near-bed flow through sparse arrays of rigid emergent vegetation. Water Resources Research, 60(4): e2023WR035879.
https://doi.org/10.1029/2023WR035879

[4] Wen, J., Chen, Y., Liu, Z., Li, M. (2022). Numerical study on the shear stress characteristics of open-channel flow over rough beds. Water, 14(11): 1752. https://doi.org/10.3390/w14111752

[5] Quick, L.A., Hoey, T.B., Williams, R.D., Boothroyd, R.J., Tolentino, P.M., David, C.P. (2025). Spatial variability in bedload transport rates determined by river pattern. EGUsphere, 2025: 1-15. https://doi.org/10.5194/egusphere-2025-2722

[6] Wang, Y., Lv, M., Wang, W.E., Meng, M. (2024). Discharge formula and hydraulics of rectangular side weirs in the small channel and field inlet. Water, 16(5): 713. https://doi.org/10.3390/w16050713

[7] Chipongo, K., Khiadani, M., Sookhak Lari, K. (2020). Comparison and verification of turbulence Reynolds-averaged Navier–Stokes closures to model spatially varied flows. Scientific Reports, 10(1): 19059. https://doi.org/10.1038/s41598-020-76128-9

[8] Maranzoni, A. (2021). Analysis of the water surface profiles of spatially varied flow with increasing discharge using the method of singular points. Journal of Hydraulic Research, 59(5): 791-809. https://doi.org/10.1080/00221686.2020.1844812

[9] Kartal, V., Emiroglu, M.E. (2022). Experimental analysis of combined side weir-gate located on a straight channel. Flow Measurement and Instrumentation, 88: 102250. https://doi.org/10.1016/j.flowmeasinst.2022.102250

[10] Chang, J., Lee, G.H., Ajama, O.D., Li, W. (2024). Estimation of bed shear stress and settling velocity with inertial dissipation method of suspended sediment concentration in cohesive sediment environments. Frontiers in Marine Science, 11: 1475565. https://doi.org/10.3389/fmars.2024.1475565

[11] Naderi, M., Afzalimehr, H., Dehghan, A., Darban, N., Nazari-Sharabian, M., Karakouzian, M. (2022). Field study of three–parameter flow resistance model in rivers with vegetation patch. Fluids, 7(8): 284. https://doi.org/10.3390/fluids7080284

[12] Mir, A.A., Patel, M. (2025). Optimizing bed shear stress prediction in open flow channels: An investigation of heuristic machine learning techniques. Natural Hazards, 121: 9103-9139. https://doi.org/10.1007/s11069-025-07154-x

[13] Mohammed-Ali, W.S., Yass, M.F., Khalaf, R.M. (2025). Novel technique for measuring erosion in riverbanks: Tigris river case at Baiji City-Iraq. Instrumentation, Mesure, Metrologie, 24(3): 207-214. https://doi.org/10.18280/i2m.240302

[14] Jamil, M.F., Ting, F.C., Kafle, M. (2025). Laboratory study of bed shear stress in gradually varied flow over a sudden change in bed roughness. Environmental Fluid Mechanics, 25(2): 15. https://doi.org/10.1007/s10652-025-10024-6

[15] Chow, V.T. (1959). Open-Channel Hydraulics. McGraw-Hill, New York. https://openlibrary.org/books/OL21345034M/Open-channel_hydraulics.

[16] Feng, D.Q., Fan, J.J., Wang, W.J., Xia, C.X., Li, A. (2024). New formula of vegetation roughness height and Darcy–Weisbach friction factor in channel flow. Journal of Hydrology, 636: 131278. https://doi.org/10.1016/j.jhydrol.2024.131278

[17] Zhao, Y., Chen, D., Qin, J., Wang, L., Luo, Y. (2024). Study on the coefficient of apparent shear stress along lines dividing a compound cross-section. Water, 16(12): 1648. https://doi.org/10.3390/w16121648

[18] Khiadani, M.H., Beecham, S., Kandasamy, J., Sivakumar, S. (2005). Boundary shear stress in spatially varied flow with increasing discharge. Journal of Hydraulic Engineering, 131(8): 705-714. https://doi.org/10.1061/(ASCE)0733-9429(2005)131:8(705)

[19] Nikushchenko, D., Pavlovsky, V., Nikushchenko, E. (2022). Fluid flow development in a pipe as a demonstration of a sequential change in its rheological properties. Applied Sciences, 12(6): 3058. https://doi.org/10.3390/app12063058

[20] Pope, S.B. (2000). Turbulent Flows. Cambridge, UK: Cambridge University Press. https://elmoukrie.com/wp-content/uploads/2022/04/pope-s.b.-turbulent-flows-cambridge-university-press-2000.pdf.

[21] White, F.M. (2015). Fluid Mechanics (8th ed.). New York, NY: McGraw-Hill. https://www.amazon.com/Fluid-Mechanics-Frank-M-White/dp/0073398276.

[22] Schlichting, H., Gersten, K. (2017). Boundary-Layer Theory (9th ed.). Berlin, Germany: Springer. https://doi.org/10.1007/978-3-662-52919-5

[23] Alfatlawi, T.J., Naji, A., Hamid, Z., Hussein, M. (2021). Grate inlet hydraulic efficiency with varying porous asphalt aprons. Journal of Irrigation and Drainage Engineering, 147(6): 04021014. https://doi.org/10.1061/(ASCE)IR.1943-4774.0001554

[24] Chang, T.H., Huang, S.T., Chen, S., Lai, J.C. (2010). Estimation of manning roughness coefficients on precast ecological concrete blocks. Journal of Marine Science and Technology, 18(2): 18. https://doi.org/10.51400/2709-6998.2331

[25] Garrote, J., González-Jiménez, M., Guardiola-Albert, C., Díez-Herrero, A. (2021). The manning's roughness coefficient calibration method to improve flood hazard analysis in the absence of river bathymetric data: Application to the urban historical zamora city centre in spain. Applied Sciences, 11(19): 9267. https://doi.org/10.3390/app11199267

[26] Nezu, I., Rodi, W. (1986). Open-channel flow measurements with a laser Doppler anemometer. Journal of Hydraulic Engineering, 112(5): 335-355.

[27] Abdulrasul, W.A., Mohammed-Ali, W.S. (2024). Experimental study of energy dissipation in sudden contraction of open channels. Instrumentation, Mesure, Metrologie, 23(1): 55-61. https://doi.org/10.18280/i2m.230105

[28] Elbeltagi, A., Vishwakarma, D.K., Katipoğlu, O.M., Sushanth, K., et al. (2025). Air temperature estimation and modeling using data driven techniques based on best subset regression model in Egypt. Scientific Reports, 15(1): 20200. https://doi.org/10.1038/s41598-025-06277-2

[29] Sobenko, L.R., Pimenta, B.D., Camargo, A.P.D., Robaina, A.D., Peiter, M.X., Frizzone, J.A. (2022). Indicators for evaluation of model performance: Irrigation hydraulics applications. Acta Scientiarum. Agronomy, 45: e56300. https://doi.org/10.4025/actasciagron.v45i1.56300

NOMENCLATURE

τ_b	Bed shear stress, M. L^{-1}. T^{-1}
u*	Friction (shear) velocity, L. T^{-1}
ρ	water density, M. L^{-3}
F	tangential (shear) force acting on the bed, M. L^{-1}. T^{-2}
A	area over which the force acts, L^2
g	gravitational acceleration, M. T^{-2}
R	Hydraulic radius, L.
S	Bed slope, dimensionless
Q	Base discharge, L^3. T^{-1}
q	Nozzle discharge, L^3. T^{-1}
V	Mean velocity, L. T^{-1}
P	Wetted parameter, L.
x	Streamwise coordinate, L.
$\Delta h/\Delta x$	Finite difference of energy grade line drop per length (head loss per unit length)

f	Darcy-Weisbach friction factor, dimensionless	y	distance from the channel bed, L
ν	Kinematic viscosity, $L^2 . T^{-1}$	u	local mean velocity at height y, $L.T^{-1}$
du/dy	Velocity gradient (rate of change of streamwise velocity with distance from wall), T^{-1}	Y^+	Express how far a point is from the wall in viscous unit, dimensionless
$\tau_\circ c$	Critical boundary shear stress, $M. L^{-1} . T^{-1}$	U^+	Express the velocity at the point in friction velocity units, dimensionless
θ_c	Critical shields parameter, dimensionless	S_L	Longitudinal slope, dimensionless
ρ_s	Sediment density, $M.L^{-3}$	$\overline{\tau_\circ}$	the average shear stress along the wetted perimeter, $M. L^{-1} . T^{-1}$
d	Particle diameter, L		
μ	dynamic viscosity of water, $M.L^{-1} . T^{-1}$		
$\tau_\circ x$	local boundary shear stress, $M.L^{-1} . T^{-1}$		